Prestack simultaneous inversion for delineation of the Lower Wilcox erosional remnant sandstone beneath the Texas Gulf Coastal Plain: A case study

Tianze Zhang[1], Yani Lin[1], Kelly H. Liu[2], and Stephen S. Gao[2]

Abstract

The Lower Wilcox lowstand sand deposits encased between two sequence boundaries along the Texas Gulf Coastal Plain are of good reservoir quality and usually gas productive. However, the sedimentation is sparsely scattered within such a depositional environment and it is hard to predict by qualitative interpretation methods. Simultaneous inversion of elastic parameters such as P-impedance, S-impedance, and density by the integration of prestack data and well logs allows us to quantitatively characterize the reservoirs and to distinguish them from the surrounding rocks. We have used prestack simultaneous inversion of the elastic parameters for delineation of the gas reservoir in an active field with limited log availabilities. For wells that are missing sonic and density logs, we estimate the parameters using the time-average equation (TAE) and Gardner's equation, respectively. The shear wave velocity estimation methods are tested and compared using the measured log value. The estimation results are verified using well-log correlations in adjacent wells. Rock-physics analyses on wells are conducted to find the optimal elastic parameters for characterizing the gas-bearing sand. We successfully delineate the reservoir using the crossplot of V_P/V_S versus S-impedance values. The inversion results are quality controlled by a producing well in the reservoir zone, and probability maps of each lithology are calculated by the probability density function. Our results from the Lower Wilcox Formation indicate that simultaneous inversion based on the estimated parameters using TAE is feasible, and the gas-bearing reservoirs can be recommended with high confidence.

Introduction

The late Paleocene Lower Wilcox Group is part of the thick sandstone/shale Wilcox sequence along the Texas Gulf Coast (Debout et al., 1982). It is mainly characterized as fluvial and deltaic deposits prograded over the mid-Cretaceous carbonate shelf margin with a high sedimentation rate (Winker, 1982; Galloway et al., 2011; Olariu and Zeng, 2017). The prograding Rockdale depositional system and abundant source supply provide favorable environments for hydrocarbon generation and preservation (Fisher and McGowen, 1969; Mackey et al., 2012; Zeng et al., 2016) (Figure 1).

The submarine canyon associated with the continental margin failure initiated with retrogressive slumping of delta-front deposits and ended with backfilling (Galloway et al., 1991). During the evolution of the canyon, sidewall slumps and sediments brought by the hyperpycnal process formed the diverse depositional facies in the canyon fill. Among all, the lower canyon sandstone facies associated with slumps and turbidites covered with backfilling mudstone are usually productive, but this is hard to predict without high-resolution 3D seismic data (Galloway and McGilvery, 1995).

Various seismic interpretation techniques have been extensively used in the Texas Gulf Coast area for stratigraphy and depositional system studies (Fisher and McGowen, 1969; Debout et al., 1982; Hargis, 1986; Galloway et al., 2000; Hargis, 2009; Olariu and Ambrose, 2016; Zeng et al., 2016; Olariu and Zeng, 2017) and structural and seismic facies analyses (Allen and Howell, 1987; McDonnell et al., 2008; Egedahl et al., 2012; Enomoto, 2014). Most of the results are based on poststack seismic attribute analyses, and the low confidence level of the results can hardly make them accurately trace the target with high confidence. Only a few studies sought to apply quantitative interpretation methods based on rock-physics analysis and seismic inversion (Wagner et al., 2012; Sarkar et al., 2016). Possible reasons for the

[1]Chengdu University of Technology, AAPG Research Center — Chengdu, State Key Laboratory of Oil and Gas Reservoir Geology and Exploitation, Chengdu, China and Missouri University of Science and Technology, Geology and Geophysics Program, Rolla, Missouri 65409, USA. E-mail: tz7t4@mst.edu; ylfw7@mst.edu.

[2]Missouri University of Science and Technology, Geology and Geophysics Program, Rolla, Missouri 65409, USA. E-mail: liukh@mst.edu (corresponding author); sgao@mst.edu.

Manuscript received by the Editor 30 August 2019; revised manuscript received 1 June 2020; published ahead of production 11 August 2020; published online 26 October 2020. This paper appears in *Interpretation*, Vol. 8, No. 4 (November 2020); p. T991–T1005, 18 FIGS.

http://dx.doi.org/10.1190/INT-2019-0178.1. © 2020 Society of Exploration Geophysicists and American Association of Petroleum Geologists. All rights reserved.

Downloaded from http://pubs.geoscienceworld.org/interpretation/article-pdf/8/4/T991/5204880/int-2019-0178.1.pdf
by Missouri University of Science and Technology user

limited application of quantitative interpretation methods include (1) prestack data acquisition is not profitable, (2) the facies and structure are usually estimated through well-log analysis, (3) insufficient log availability impedes the use of a more accurate quantitative method such as prestack seismic inversion, and (4) there are limited publications due to data confidentiality.

The simultaneous inversion process applied in this study inverts the prestack seismic data into different elastic volumes and reduces the interpretation ambiguity caused by solely inverting for the P-impedance volume (Hampson et al., 2005; Russell and Hampson, 2006). By quantifying the properties of the reservoir using well-log analysis, we can delineate and quantify the risk of the gas-bearing sandstone area with high confidence. A successful inversion process requires a comprehensive set of log types, especially the density and velocity information, for accurate seismic-to-well correlation and elastic parameter calculation. However, those logs are not always available; hence, wisely choosing and verifying the log estimation method is crucial for the inversion results.

This study focuses on the interchannel erosional remnant sand reservoir within the canyon fill (Figure 2). The objective is to test the log estimation method in the Lower Wilcox Formation and to explore the feasibility of accurately performing the prestack inversion method in the reservoir field that lacks essential velocity and density information. We use a data set acquired from an active field that contains a 3D seismic survey and well logs. For wells missing the P-wave velocity and density, we estimate these values using the time-average equation (TAE) and lithology specific Gardner's equation, respectively. The estimation results are tested and verified on two testing wells before applying the method to other wells for the inversion. A clear separation of the pay sand section from the background trend is observed in the well-log analysis, and the results are used to quantify the properties of the reservoir and later describe the reservoir extent using the inverted results. The accuracy of the results is examined by a producing well drilled in the field. Besides, the probability density function allows us to calculate the probability for each lithology and quantify the risk of the predicted area. The promising results from this study suggest that the same workflow and method can be applied to similar regions in the Lower Wilcox Formation.

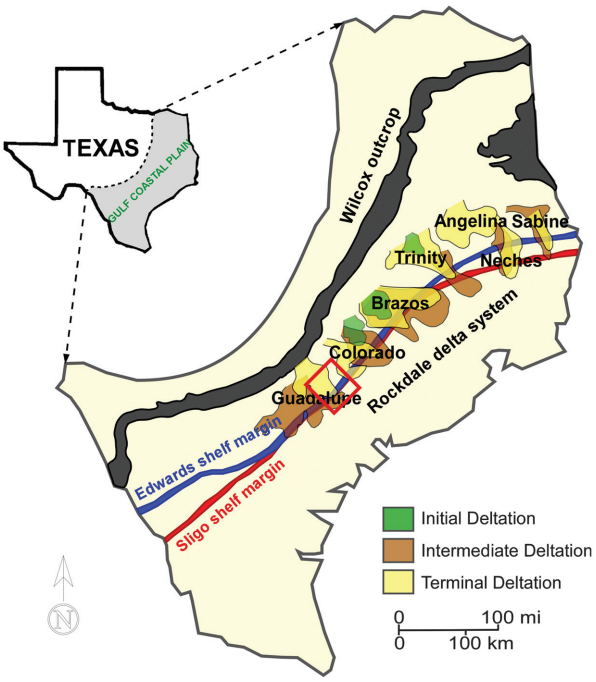

Figure 1. Location of the Texas Gulf Coast (modified from Olariu and Zeng, 2017). The study area is indicated by the red rectangle.

Data and method

Seismic and well data

A 3D prestack seismic data set that covers an area of 9.3 square miles and logs from eight wells are used in the inversion process (Figure 3). The seismic survey contains 166 inlines and 261 crosslines with offset ranging from 1000 to 19,000 ft. The main frequency ranges from 10 to 40 Hz, with a dominant frequency of approximately 28 Hz. Preconditioning of the prestack seismic data is essential to obtain reliable inversion results (Zhang et al., 2014); thus, the data set is processed

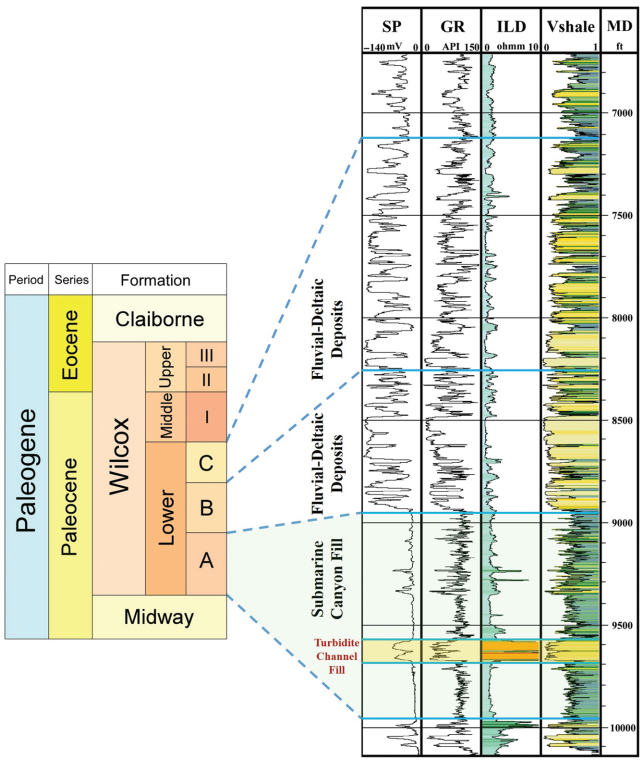

Figure 2. Stratigraphy of the Lower Wilcox Formation and well logs of well-3. The light-green color in the Lower Wilcox A shows the submarine canyon fill. The smaller values in the V_{shale} column are in yellow and correspond to sandstone, and the larger values are in blue and correspond to shale.

Downloaded from http://pubs.geoscienceworld.org/interpretation/article-pdf/8/4/T991/5204880/int-2019-0178.1.pdf
by Missouri University of Science and Technology user

by normal moveout procedure and muted to increase the signal-to-noise ratio by reducing the noise from distant common-depth-point gathers. The preprocessed data set is transformed into angle gathers for further inversion processing.

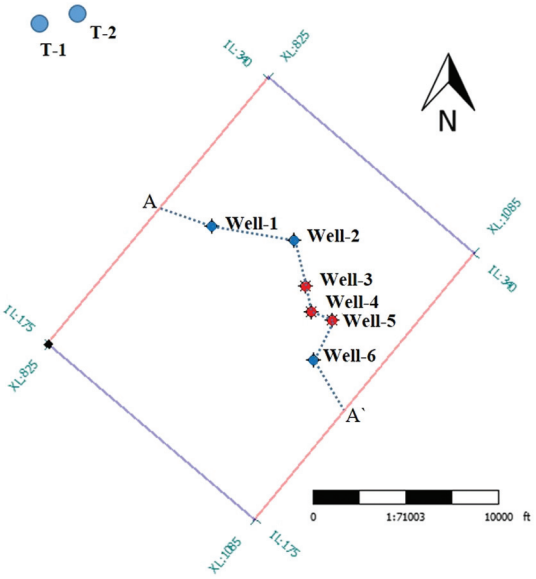

Figure 3. Basemap showing the seismic and well locations. The dashed blue line displays the location of the arbitrary line A-A'.

Six of the eight wells are located within the survey area. Two producing wells (well-3 and well-4) that penetrate the same pay sand interval with greater than 80 ft thickness are used for rock-physics and inversion analyses of the sandstone reservoir. Three dry wells (well-1, well-2, and well-6) provide constraints on the inversion process, and a producing well (well-5) is used to test the accuracy of the results. The log type for wells within the seismic survey is limited: Only gamma ray, spontaneous, resistivity, and conductivity logs are available (Figure 4), whereas the essential logs for the inversion process include density, sonic, and shear wave velocity logs. Although there are numerous empirical equations that describe the relations between resistivity, velocity, and density, choosing inappropriate relations can significantly affect the credibility of the inversion results. In this study, the performance of the density and velocity estimation method is tested using two wells (T-1 and T-2), which contain full log types and are located adjacent to the seismic survey.

Key log estimation

Sonic and density logs are the most crucial data for seismic-to-well tie and prestack inversion. Because both logs are missing from the wells within the seismic area, in this study, we estimate the P-wave velocity from resistivity logs first, and then we calculate the density log from the velocity estimation.

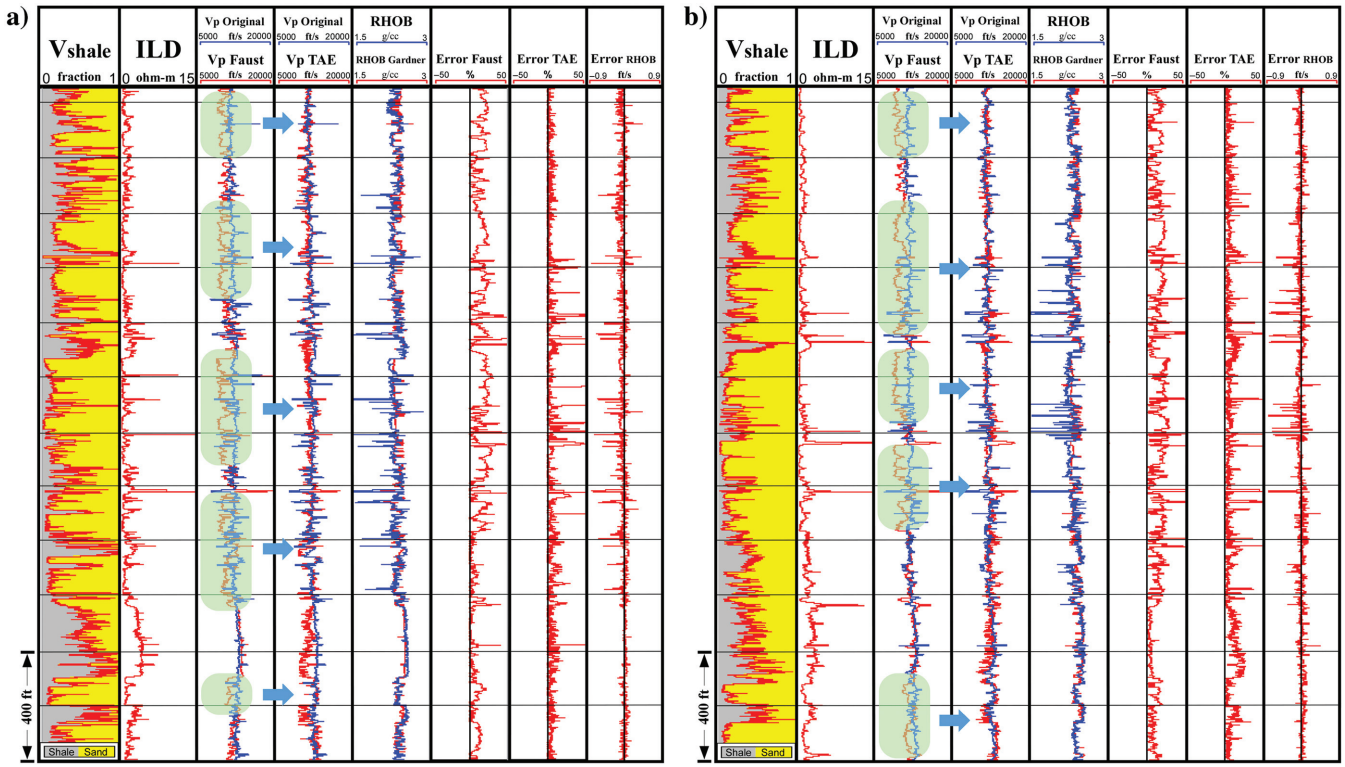

Figure 4. Example logs used in the velocity and density estimation and a comparison between the estimated (blue) and calculated logs (red). The areas in cyan are the zones with significant errors using Faust's estimation. The calculated errors are the absolute values of the relative errors to the original logs and are significantly reduced in the TAE estimation. The shale volume (V_{shale}) log is calculated by the gamma-ray and resistivity (ILD) logs. (a) Well T-1 and (b) well T-2.

Downloaded from http://pubs.geoscienceworld.org/interpretation/article-pdf/8/4/T991/5204880/int-2019-0178.1.pdf
by Missouri University of Science and Technology user

Empirical equations such as Faust's equation describe the relationship between the P-wave velocity and resistivity, but the estimation results are usually unstable and cannot be applied in areas with different lithology conditions such as the Lower Wilcox Formation, which is dominantly composed of sandstone and mudstone. This study uses TAE to estimate the sonic log from resistivity log. TAE takes the lithology difference and formation porosity into account, and quantifies its effectiveness in comparison with other empirical equations (Adcock, 1993). TAE for the two-lithology matrix form is given by

$$\Delta T = \Delta T_F f_R + [\Delta T_{sh} f_{sh} + \Delta T_{sd}(1 - f_{sh})](1 - f_R), \quad (1)$$

where ΔT_F, ΔT_{sh}, and ΔT_{sd} are the sonic travel times for fluid, shale, and sand, respectively. The fractional shale volume (f_{sh}) is calculated by the gamma-ray log. The fractional porosity (f_R) is calculated by Archie's equation, which assumes that the sand is fully saturated with water, using

$$f_R = (aR_w/S_w^n Rt)^{1/m}, \quad (2)$$

where the constants a, n, and m are 0.81, 2, and 1, respectively. The R_w values are estimated from the mud filtrate and drill mud resistivity acquired from log heading. The R_w value for the two producing wells is 0.035 Ω-m for well-3 and 0.03 Ω-m for well-4. The water saturation value is estimated at 20% for the gas-bearing zone, which is the average value in the testing wells. The gamma-ray and resistivity logs are normalized before calculating the shale volume and porosity to reduce the error caused by the logging devices or measurements.

Lithology-specific Gardner's equations for the sandstone and shale are then used for the bulk density estimation, which are given by

$$f_{sh} < 0.25 : \rho_b = -0.0115 V_P^2 + 0.261 V_P + 1.515, \quad (3)$$

$$f_{sh} > 0.25 : \rho_b = -0.0261 V_P^2 + 0.373 V_P + 1.458. \quad (4)$$

The P-wave velocity and density estimation methods are tested in well T-1 before being applied to the other wells for inversion. The velocity and density values calculated by TAE and Gardner's equation are compared with the measured values, and the P-wave estimation results by Faust's equation are also compared with results from TAE (Figure 4a). The results suggest that the missing parameters are accurately estimated and that the performance of TAE is better than Faust's equation with significantly lower errors. The equations with identical parameters are applied to another testing well T-2 for quality control (Figure 4b). The results demonstrate that the errors in P-wave estimation by Faust's equation are greatly reduced by the TAE, and the errors in density estimation by Gardner's equation are also in a tolerable range. The seismic-to-well-tie process is one of the key steps in the interpretation workflow, and it cannot be achieved without knowing the time-depth correlation that is provided by either check-shot data or P-wave velocity. The tying process for the testing wells is conducted by the original logs and the estimated logs, and the correlation quality can be visually checked by matching the synthetic seismogram to the extracted seismic trace. The computed seismogram using the estimated logs matches a major part of the seismic trace with a similar amplitude and peak/trough waveform pattern (Figure 5). The slight reduction in correlation coefficients is caused by the dissimilarity of amplitude in a few locations. The overall good correlations in the test wells indicate high accuracy in the estimation and that the methods are qualified to be applied in the wells for inversion.

After calculating the sonic and density logs, seismic-to-well-tie process is conducted for all of the wells to match the well-log information to the seismic, guided by the interpreted horizons. Figure 6 shows log correlation results from the two producing wells in the study area. A 28 Hz Ricker wavelet with a 100 ms time length is used. The correlation coefficient within the Lower Wilcox Formation is 0.419 for well-3 and 0.436 for well-4. The values are acceptable considering that the wells containing both logs only have correlation coefficients ranging from 0.5 to 0.6 for well T-1 and T-2 in the nearby field. The good match in waveform patterns and amplitude between synthetic seismogram and seismic trace represents a good estimation on the density and velocity logs for the Lower Wilcox Formation.

The shear wave velocity (V_S) is another key component in seismic inversion. We test and compare various *V*s estimation methods in well T-2, which is the only well that contains shear-wave measurements. The water-saturated V_P-V_S relation based on clay content (Han et al., 1986) is given by

$$f_{sh} < 0.25 : V_S = 0.754 V_P - 0.657, \quad (5)$$

$$f_{sh} > 0.25 : V_S = 0.842 V_P - 1.099. \quad (6)$$

For the gas-saturated zone, we applied Krief's equation (Krief et al., 1990), which is given by

$$V_S = \sqrt{\frac{V_P^2 - 0.902}{2.282}}. \quad (7)$$

Rock-physics analysis

Rock-physics analysis is performed on wells to find the optimal elastic parameters to characterize the reservoir. For this purpose, we crossplot the S-impedance with V_P/V_S ratio in the Lower Wilcox Formation to characterize the reservoir (Figure 7a). The analysis of data points from five wells shows a distinct separation between two clusters of data, a cluster on the left side

Downloaded from http://pubs.geoscienceworld.org/interpretation/article-pdf/8/4/T991/5204880/int-2019-0178.1.pdf
by Missouri University of Science and Technology user

with a low V_P/V_S ratio and a slightly higher S-impedance value, and a cluster showing the background trend of the rest of the data. The left cluster is equivalent to the pay sand sections in well-3 and well-4 (Figure 7b). On the crossplot of V_P/V_S and S-impedance (Figure 7a), the pay sand is marked by an irregularly shaped region. The V_P/V_S values in the region range from 1.55 to 1.65, and the S-impedance values range from 12,500 to 21,500 (ft/s)*(g/cm^3). The crossplot shows that both parameters should be used to characterize the reservoir, whereas using a single parameter can cause ambiguity in the inversion results.

Prestack simultaneous inversion

The prestack simultaneous inversion method proposed by Hampson et al. (2005) derives the elastic parameters from the prestack PP angle gathers. The method is based on Fatti's reformulation of the Zoeppritz's equation (Fatti et al., 1994), which is given by

$$T(\theta) = A_1 W(\theta) D L_P + A_2 W(\theta) D \Delta L_S + c_3 W(\theta) D \Delta L_D, \tag{8}$$

where

$$A_1 = \frac{1}{2}(1 + \tan^2\theta) + \frac{1}{2}k\left(-8\left(\frac{V_S}{V_P}\right)^2 \sin^2\theta\right) + m\left(2\left(\frac{V_S}{V_P}\right)^2 \sin^2\theta - \frac{1}{2}\tan^2\theta\right), \tag{9}$$

$$A_2 = \frac{1}{2}\left(-8\left(\frac{V_S}{V_P}\right)^2 \sin^2\theta\right), \tag{10}$$

$$W(\theta) = \text{wavelets dependent on incident angle } \theta, \tag{11}$$

$$L_P = \ln(Z_P), \tag{12}$$

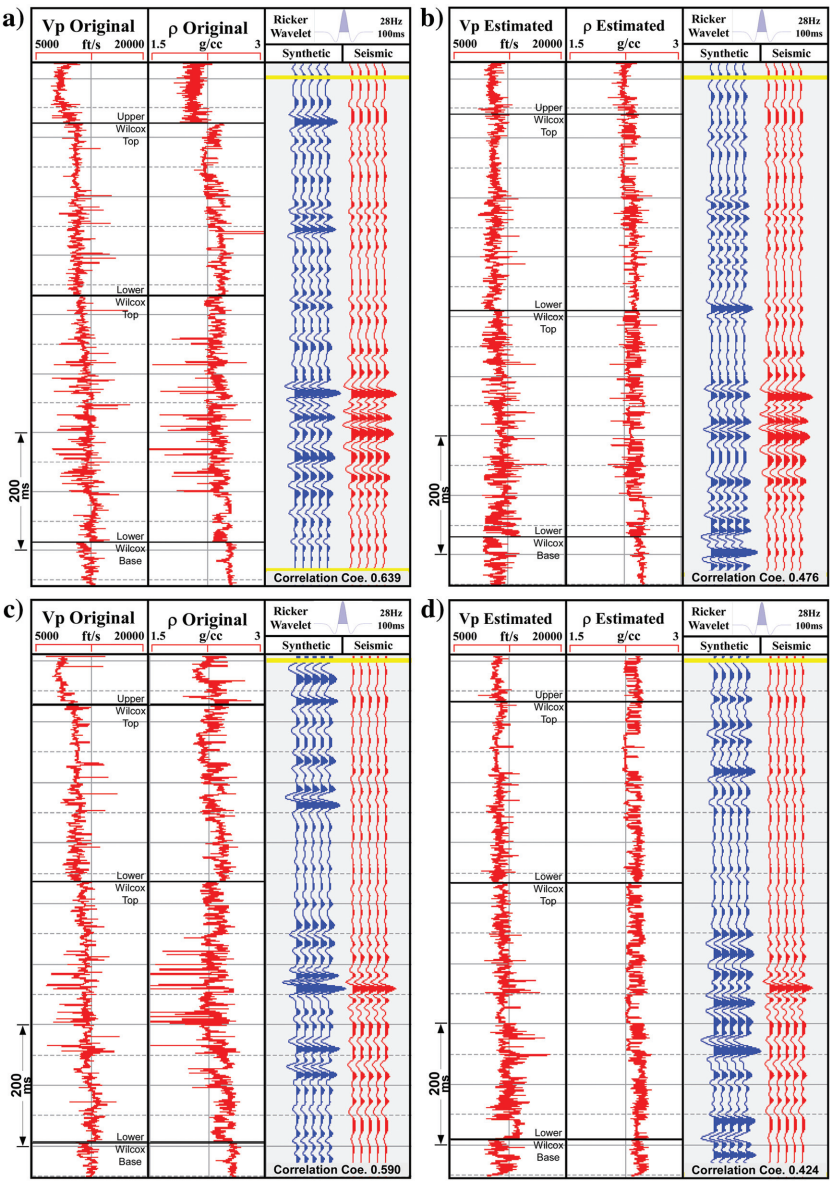

Figure 5. A comparison of the seismic to well tie in well T-1 and well T-2. The yellow lines represent boundaries used to calculate the correlation coefficients. (a) Well T-1 with the original velocity and density, (b) well T-1 with the estimated velocity and density, (c) well T-2 with the original velocity and density, and (d) well T-2 with the estimated velocity and density.

Downloaded from http://pubs.geoscienceworld.org/interpretation/article-pdf/8/4/T991/5204880/int-2019-0178.1.pdf
by Missouri University of Science and Technology user

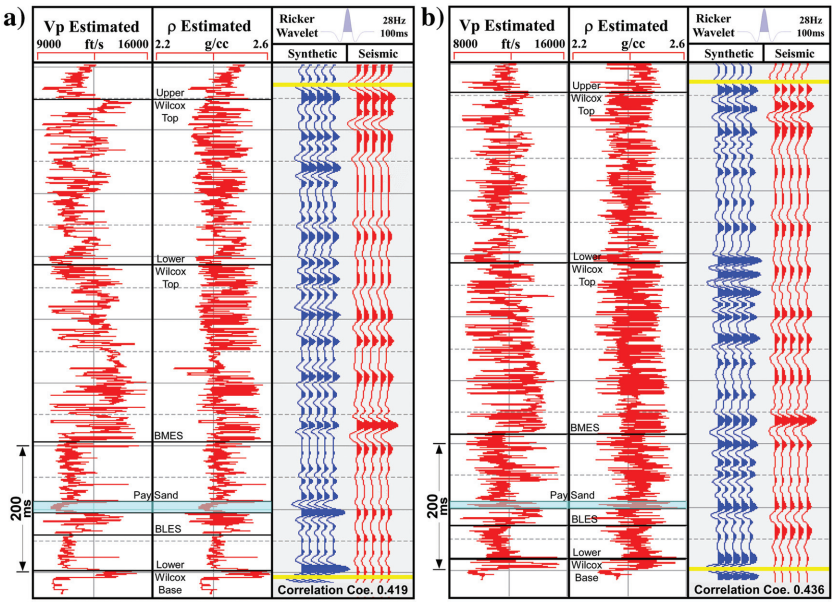

Figure 6. Log correlation results of well-3 and well-4 using the estimated velocity and density logs. BMES, base of the middle erosional sequence; BLES, base of the lower erosional sequence. (a) Well-3 and (b) well-4.

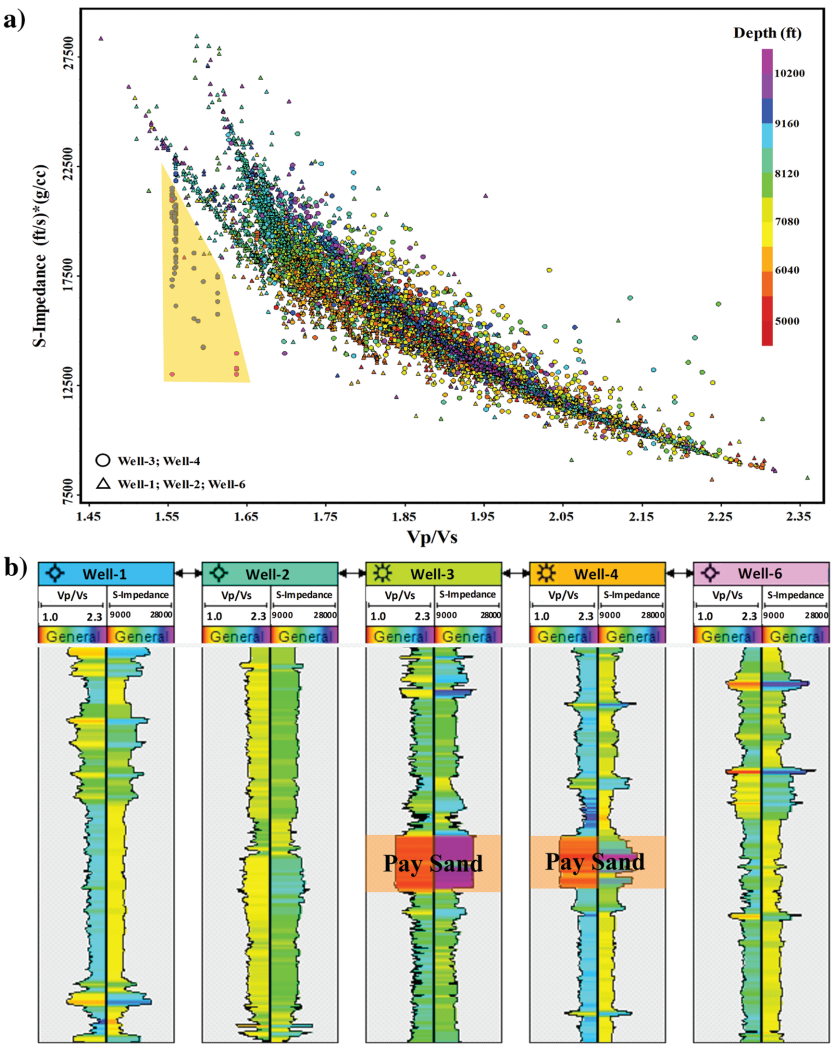

Figure 7. (a) Results of the rock-physics analysis. The yellow-colored area is equivalent to the colored sections in (b), which represents the pay sand location. (b) Cross section for each of the five wells. The logs are filled with a rainbow palette. The pay sand locations in well-3 and well-4 are colored orange.

Downloaded from http://pubs.geoscienceworld.org/interpretation/article-pdf/8/4/T991/5204880/int-2019-0178.1.pdf
by Missouri University of Science and Technology user

$$Z_P = \text{P impedance}. \tag{13}$$

The variables k, m, ΔL_S, and ΔL_D can be calculated from the following linear relations:

$$\ln(Z_S) = k \ln(Z_P) + k_c + \Delta L_S, \tag{14}$$

$$\ln(\rho) = m \ln(Z_p) + m_c + \Delta L_D, \tag{15}$$

where k and m are calculated by using the least-squares method. In this study, the best fit k and m are 1.48005 and 0.166301, respectively. The inversion process requires a set of angle gathered traces and a group of wavelets varied in incident angles as inputs. We convert the conditioned prestack data to angle gathers that range from 1 to 40°. Two angle-dependent stationary wavelets are statistically extracted from the angle gather volume: One has an angle range of 1°–20°, and the other has an angle range of 21°–40° (Figure 8).

Another essential input for the inversion process is the low-frequency geologic model, which compensates the low-frequency component that is absent in band-limited seismic data. In this study, we tested different initial models including a low-frequency model. The model built with density and computed impedance of log data was selected as an initial input to constrain the inversion process. The sections between wells are interpolated laterally and are guided by the interpreted horizons. In this study, the model consists of the computed Z_P, Z_S, the density logs of five wells, and eight horizons traced along the layers (Figure 9).

Results and discussions

Inversion and analyses

To ensure quality, it is critical to conduct analyses for the inversion results from real data before applying the inversion method to the whole volume. Well-3 and well-4 show a good correlation between the inverted and original logs, especially for the pay sand zone, where V_P/V_S and S-impedance show distinct values from the surrounding layers (Figure 10). The mismatch in the 50 ms time window below top of the middle erosional sequence (TMES) is a result of the interbedded thin layer. Although the inverted elastic parameters in the window may not reflect the thin layers accurately, the general trend matches well with the computed log values and the inversion of the pay sand zone is not affected.

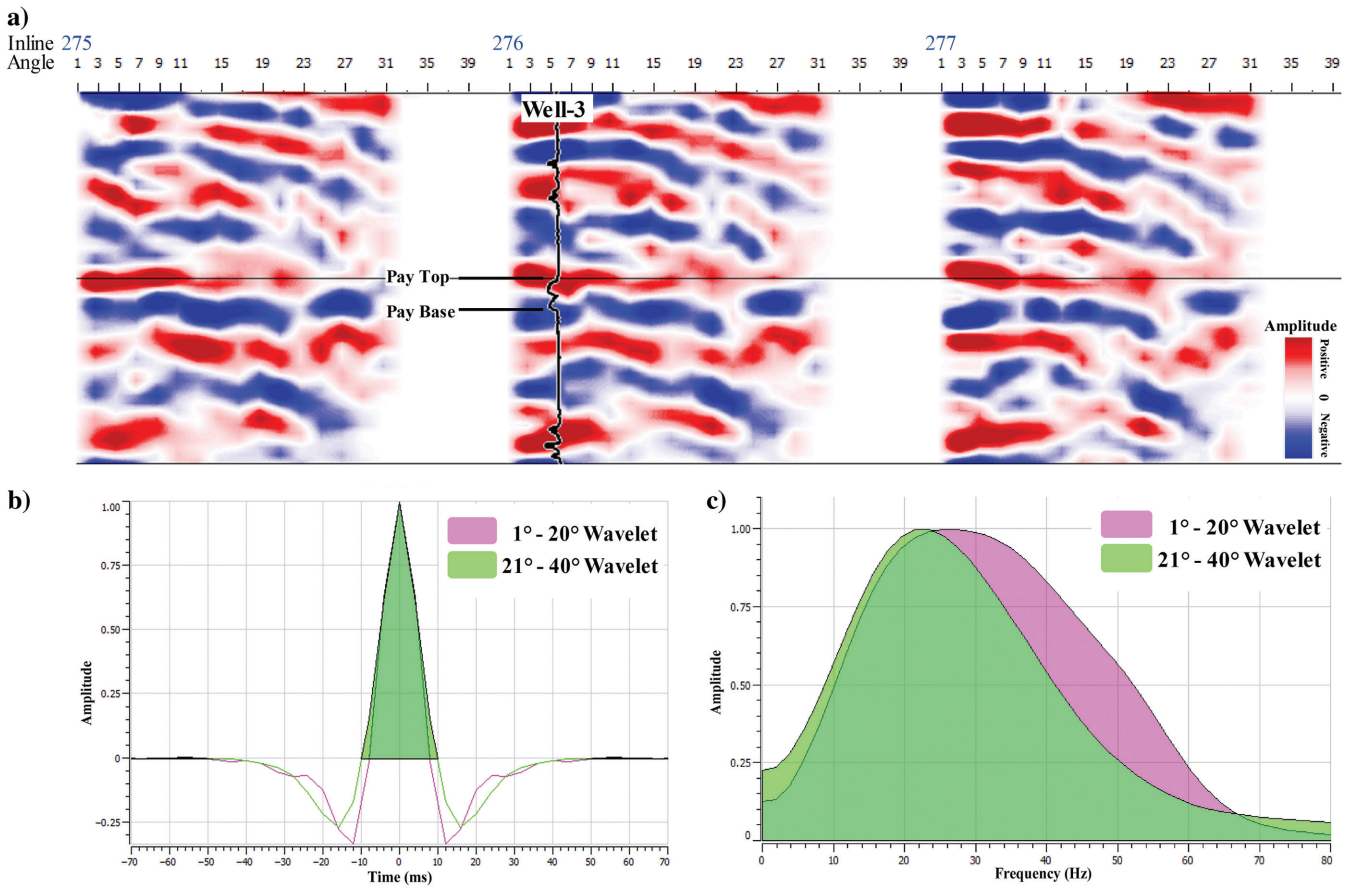

Figure 8. Example of prestack angle-gather profiles near well-3, which focuses on the pay sand location, and wavelets extracted from the angle-gather volume. The Angle ranges from 1° to 20° (pink), and 21° to 40° (green) in the time domain and frequency domain: (a) Prestack angle-gather profiles. The wider angles are in the deeper formation. (b) Wavelets in the time domain and (c) wavelets in the frequency domain.

Downloaded from http://pubs.geoscienceworld.org/interpretation/article-pdf/8/4/T991/5204880/int-2019-0178.1.pdf
by Missouri University of Science and Technology user

The simultaneous inversion algorithm is applied to the entire data volume, as shown along the arbitrary profile A-A' crossing all six wells (Figure 11). The reservoir area is bounded by well-2 in the north and well-6 in the south. The S-impedance and V_P/V_S attributes show significant anomalies, whereas the P-impedance attribute shows normal values. The significantly high S-impedance and low V_P/V_S represent a possible gas-saturated zone, but the exact extent of the area cannot be determined with confidence because similar anomalies can also be observed in the up- and downdipping regions as marked by the arrows in Figure 11b and 11c.

To map the reservoir area, we crossplot the inverted V_P/V_S volume versus the inverted S-impedance volume (Figure 12), similar to the rock-physics analysis conducted on wells. The volume data show no distinctive cluster of gas sand and background trend. An area is selected using the range obtained from the analysis of nearby wells (Figure 7), where the V_P/V_S ranges from 1.5 to 1.65 and the S-impedance ranges from 16,000 to 21,500 (Figure 12). The cross section provides better isolation for the sand body than individual parameters. Among all five wells used for the inversion, the production wells, well-3 and well-4, are drilled at the predicted reservoir location from the inversion, and the rest are outside of the area (Figure 13). The base of the lowest sequence boundary (BLES) is traced along the incised canyon beneath the gas-bearing sand body (Figure 13). The structure of the canyon shows a general dipping direction from northwest to southeast, and the mass transported by the distributary channels feeds the lower section with sandy turbidites. The sandstone reservoir was transported from the updip region through the steep canyon wall, and then it was trapped at the canyon floor (Figure 13).

The main reservoir body and an elongated area in the northeast are analyzed in detail (Figure 14). The thickness of the pay sand decreases from well-3 to well-5, which is consistent with their production rates (Figure 14a). The possible reservoir area dips from northwest to southeast as shown in the time structure map, following the same direction of the mass wasting inside the canyon system (Figure 14b).

The producing well, well-5, is used for testing the accuracy of the inversion result (Figure 15). The traces from each inverted attribute volume are extracted from

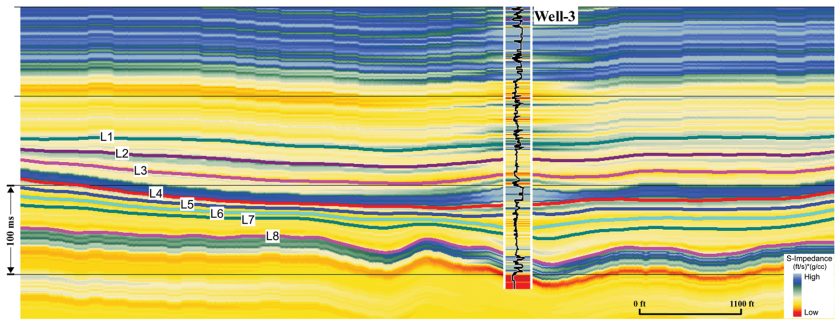

Figure 9. The S-impedance model of a crossline intersecting well-3. A high value of S-impedance is observed at the pay sand layer between L3 and L4.

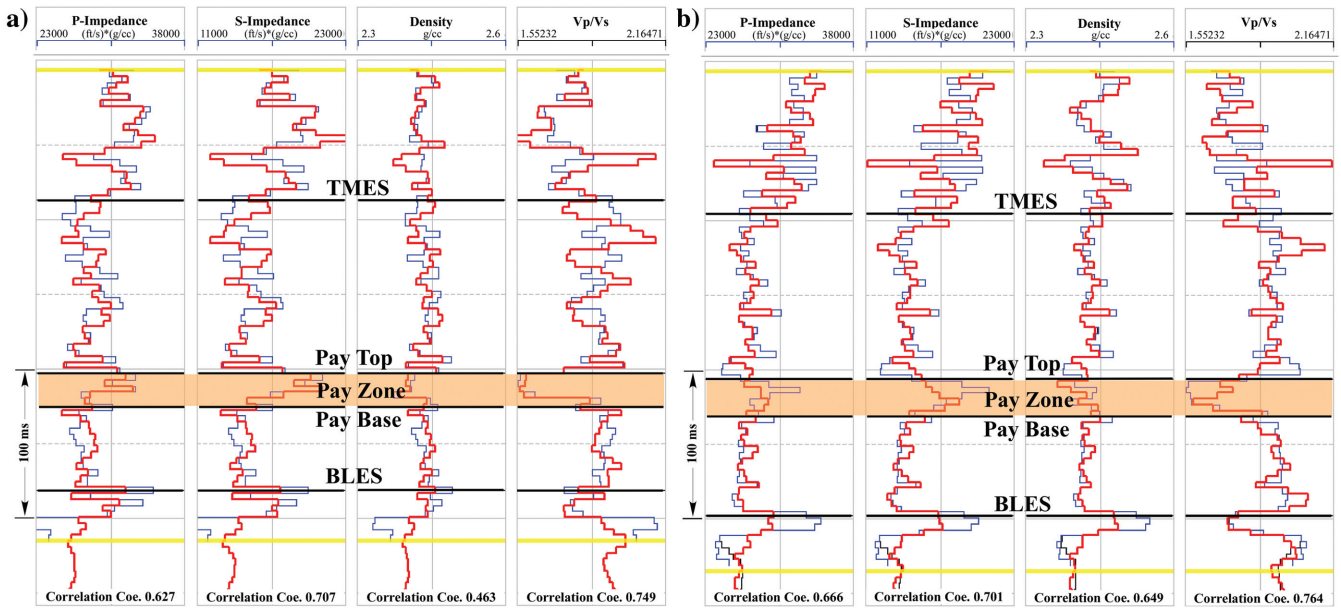

Figure 10. Inversion analyses for well-3 and well-4. The log panels from left to right are the P-impedance, S-impedance, density, and V_P/V_S. The original logs are in blue, and the inverted logs are in red. TMES, top of the middle erosional sequence; BLES, base of the lower erosional sequence. (a) Well-3 and (b) well-4.

Downloaded from http://pubs.geoscienceworld.org/interpretation/article-pdf/8/4/T991/5204880/int-2019-0178.1.pdf
by Missouri University of Science and Technology user

the well location and overlapped with the computed logs. The error is calculated by subtracting the inverted values from the computed ones. The error analysis results suggest that the parameters of the simultaneous inversion are reliable and can be used for reservoir characterization with confidence. The reservoir area, which is represented by high S-impedance and low V_P/V_S, correlates well with the pay sand zone in well-5, confirming the reliability of the inversion results (Figure 15).

Lithology classification

As shown in Figure 12, no distinction of the gas sand cluster is observed in the crossplot of the inverted attributes, which indicates that errors may exist when picking the cross section using the parameter from the well analysis. The Bayesian kernel density estimation is used to calculate the probability density for each lithology class to reduce such error. Using data from five wells, we classify the lithology into gas sand, wet sand, and shale based on the criteria of resistivity and shale volume, and birvariate kernel density estimation is applied to each class in the V_P/V_S and S-impedance domain to calculate the probability density distribution (Figure 16). The contours in different colors stand for the probability distribution of each class. The probability gradually decreases toward the outside of the circle.

The density function is then applied to the inverted data volume of the V_P/V_S and S-impedance, and each

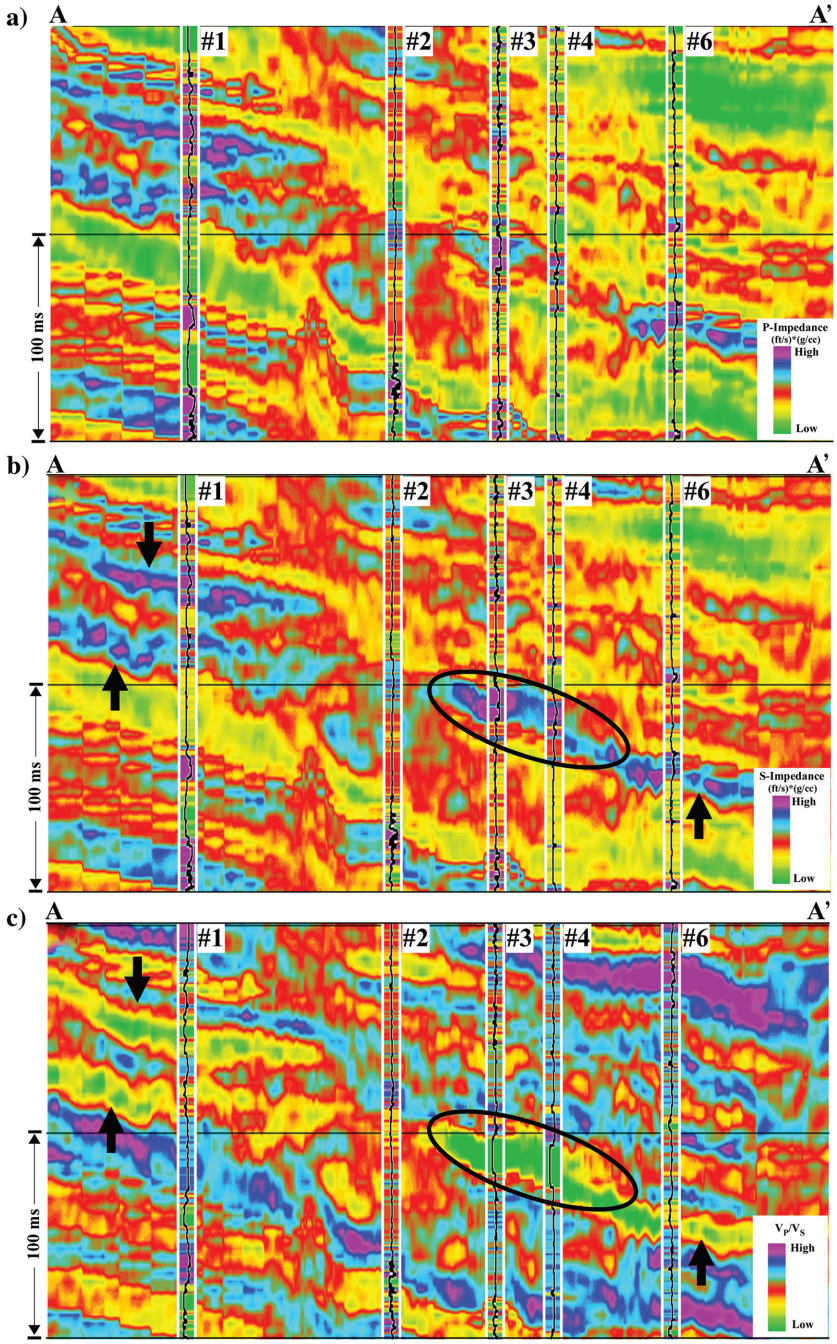

Figure 11. Inverted elastic attributes along profile A-A'. The ellipses indicate the reservoir zone represented by low V_P/V_S and high S-impedance values. The arrows mark the zone with similar anomalous values as the reservoir. (a) P-impedance, (b) S-impedance, and (c) V_P/V_S.

Downloaded from http://pubs.geoscienceworld.org/interpretation/article-pdf/8/4/T991/5204880/int-2019-0178.1.pdf
by Missouri University of Science and Technology user

class with a probability higher than 50% is displayed (Figure 17). The possible gas-saturated area is highlighted with a probability higher than 90% (Figure 17a). The water-saturated zones around well-1 and adjacent to well-6 correspond to the zone observed from the inverted elastic attribute volume (Figure 11), which shows similar anomalous values caused by the reservoir.

The extracted gas sand volume is compared with the cross section picked from well analysis (Figure 18). Most of the area is overlapped with a probability that is higher than 90%. This demonstrates the high accuracy of the inversion results and suggests that other potential gas prospects can be identified with high confidence. The elongated region on the northeast with high gas sand probability of the study area is a highly recommended area for future exploration, which has moder-

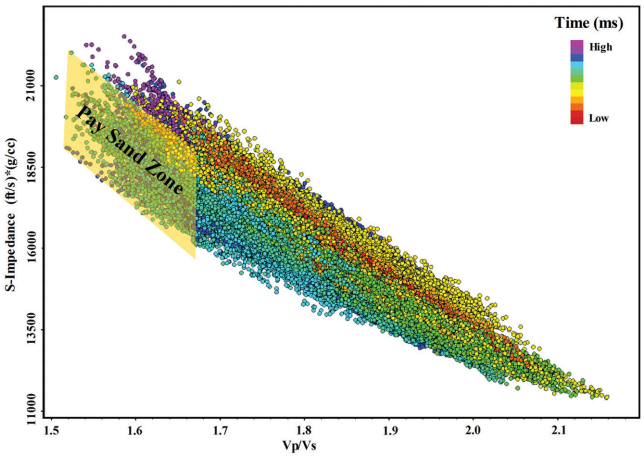

Figure 12. Inverted S-impedance versus V_P/V_S values.

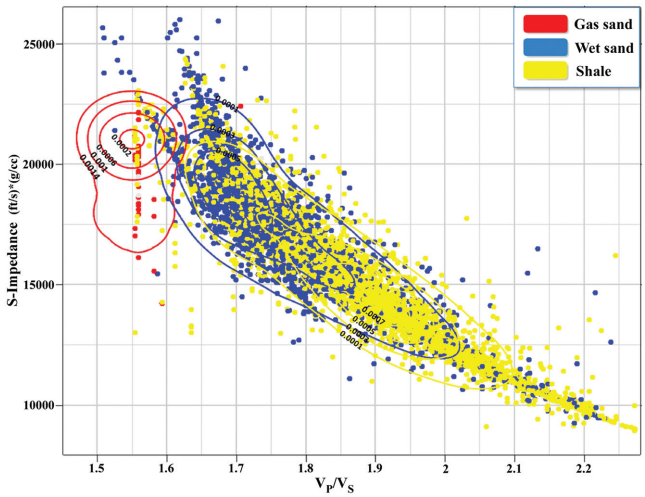

Figure 16. Density map of each lithology class calculated by the kernel density estimation.

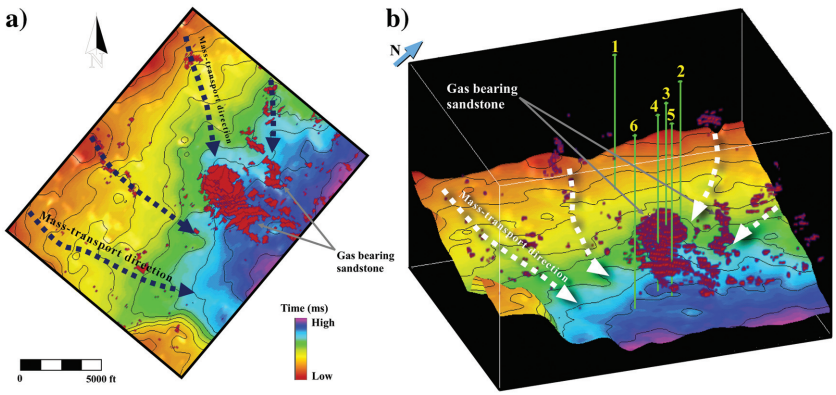

Figure 13. Inverted gas-bearing sand and the incised canyon boundary. The dashed arrows represent the location of submarine distributary channels that transport the mass into the middle canyon area. (a) Plane view and (b) 3D view.

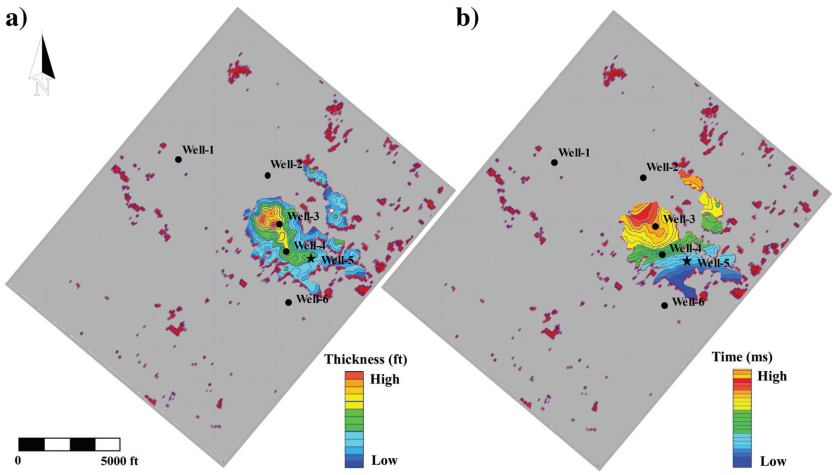

Figure 14. Plane view of the isolated pay sand area. (a) Isopach map and (b) structure map.

Downloaded from http://pubs.geoscienceworld.org/interpretation/article-pdf/8/4/T991/5204880/int-2019-0178.1.pdf
by Missouri University of Science and Technology user

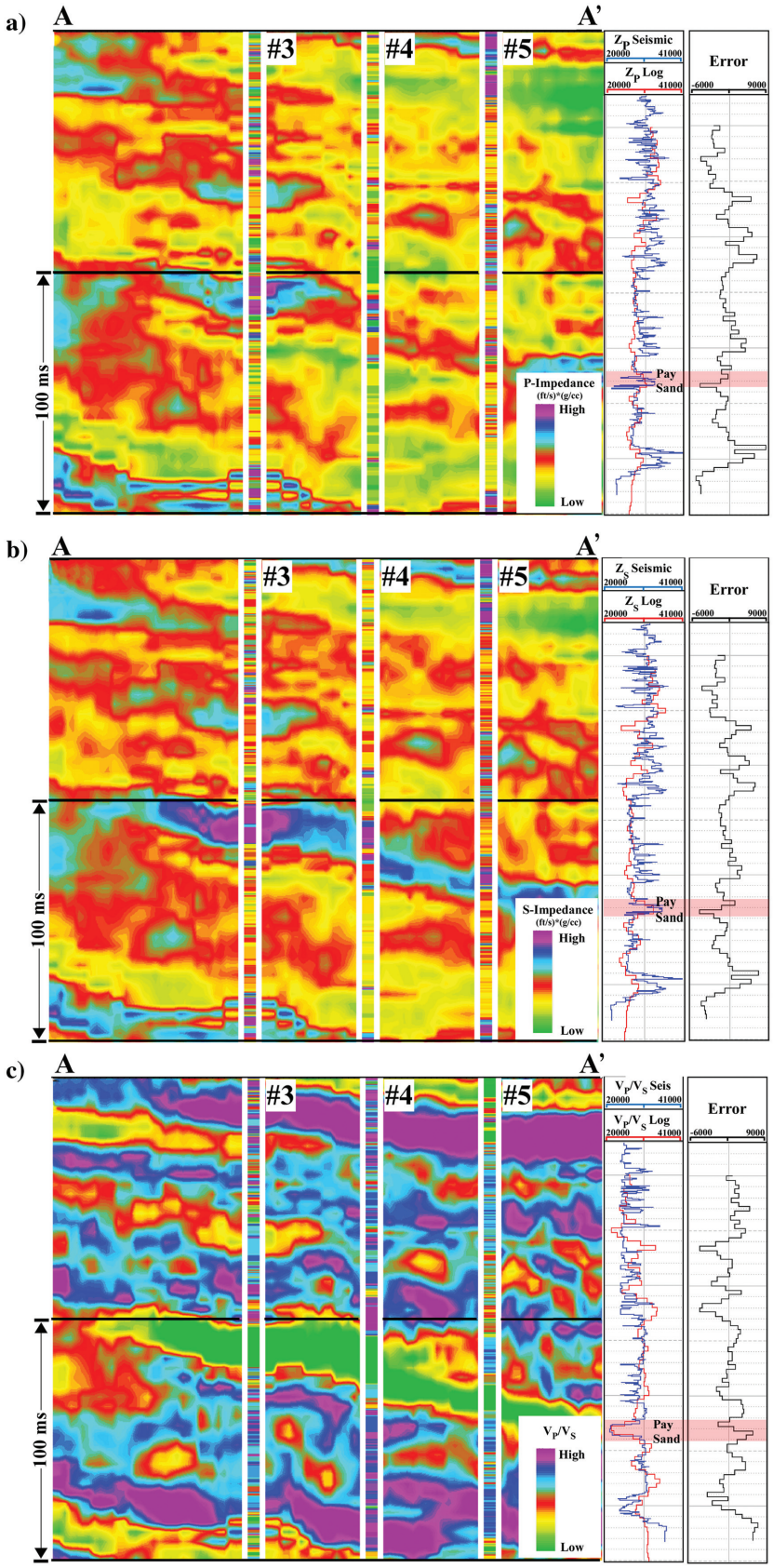

Figure 15. Inversion quality control with well-5 along A-A', by overlapping the computed logs (blue) with the inverted values (red). (a) P-impedance, (b) S-impedance, and (c) V_P/V_S ratio.

Downloaded from http://pubs.geoscienceworld.org/interpretation/article-pdf/8/4/T991/5204880/int-2019-0178.1.pdf
by Missouri University of Science and Technology user

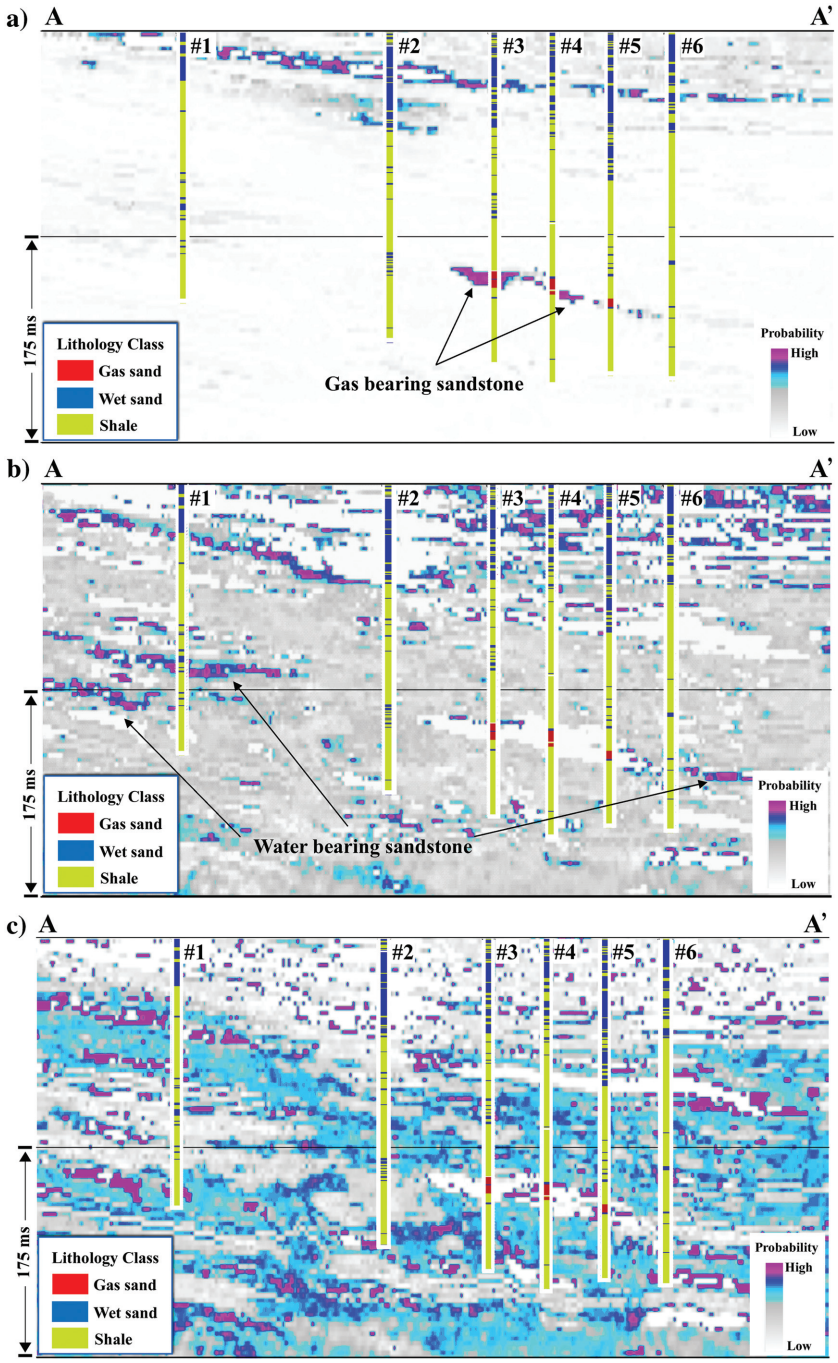

Figure 17. Probability map of each lithology class. (a) Gas sand, (b) wet sand, and (c) shale.

ate thickness and the same dipping direction as the main body.

Importance of simultaneous inversion

Isolation is one of the major characteristics of the interchannel sandstone reservoir in the study area. As a result, the extent of the reservoir is limited, and even a tight well placement can miss the prospect (e.g., well-2 and well-6). Determination of the location of a prospective reservoir can be misled in traditional acoustic inversion of Z_P alone. As indicated in this study, well-1 and well-6 were drilled in areas with similar P-impedance, S-impedance, and V_P/V_S values in the up- and downdip regions of the reservoir (Figure 11), which indicate water-saturated sandstones based on the inversion parameters (Figure 17b). Simultaneous prestack inversion of various elastic attributes can provide additional constraints to hydrocarbon exploration and lithology classification. Accurate quantitative seismic analysis using multiple elastic parameters is necessary to predict the distribution and geometry of the reservoir. This study demonstrates that even in areas with sparse well control and limited log availability, the prestack inversion procedure presented here can still produce reliable results. The errors in the estimation process can be restricted in a small range by properly choosing the estimation method and testing its effectiveness in the local field.

Downloaded from http://pubs.geoscienceworld.org/interpretation/article-pdf/8/4/T991/5204880/int-2019-0178.1.pdf
by Missouri University of Science and Technology user

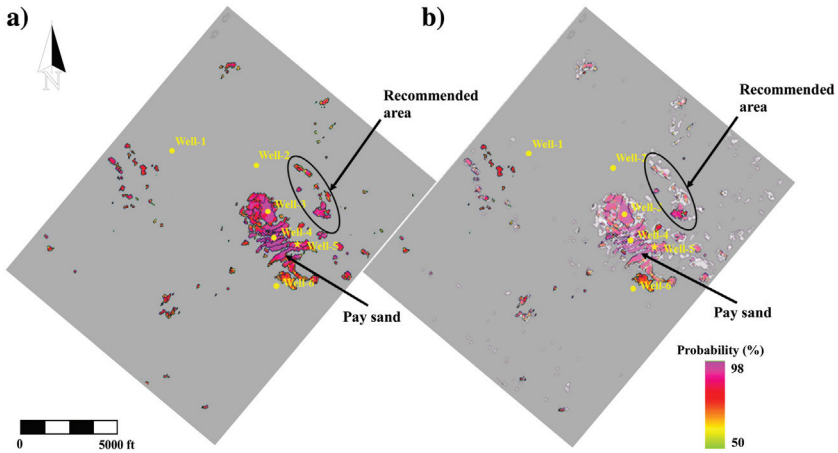

Figure 18. Top view of the gas sand probability map and comparison with the estimated result from Figure 12. (a) Gas sand probability and (b) estimated sand body overlapped with probability.

Conclusion

This study applies prestack seismic inversion using the estimated velocity and density logs to an active field beneath the Texas Gulf Coastal Plain with a focus on the Lower Wilcox gas-bearing sand formation. The analyses indicate that the TAE can provide a better estimation on velocity than the empirical Faust's equation in the Lower Wilcox Formation. The calculated velocity is used to estimate the density by Gardner's equation and to accurately conduct the seismic-to-well-tie process. The simultaneous inversion results using the estimated values are accurate, and the quality is tested by a producing well. Based on the probability density function, the probability of each lithology is calculated with high confidence. The reservoir area is delineated, and the morphology is indicated by the inverted volumes. The study suggests that the estimated velocity and density using the time average and Gardener's equations are accurate for the Lower Wilcox Formation and that the seismic inversion results based on the estimated parameters are reliable. The same workflow and approach can be applied to other fields similar to the Lower Wilcox Formation for hydrocarbon exploration and depositional facies recognition and delineation.

Acknowledgments

We are thankful to a generous company for donating the comprehensive data set used in this study. Careful reviews by the associate editor B. Zhang and four anonymous reviewers significantly improved the manuscript. We would also like to thank CGG and IHS Markit for the generous donations of the Hampson Russell and Kingdom software packages.

Data and materials availability

Data associated with this research are confidential and cannot be released.

References

Adcock, S., 1993, In search of the well tie: What if I don't have a sonic log?: The Leading Edge, **12**, 1161–1164, doi: 10.1190/1.1436929.

Allen, J., and J. Howell Sr., 1987, Using "poor man's 3-D" to identify distributary channel sands in the Wilcox formation, Lavaca County, Texas: The Leading Edge, **6**, 8–15, doi: 10.1190/1.1439339.

Debout, D. G., B. R. Weise, A. R. Gregory, and M. B. Edwards, 1982, Wilcox sandstone reservoirs in the deep subsurface along the Texas Gulf Coast: Their potential for production of geopressured geothermal energy, Report of Investigations No. 117 (No. DOE/ET/28461-T2), Texas Univ., Austin (USA), Bureau of Economic Geology.

Egedahl, K., G. L. Kinsland, and D. Han, 2012, Seismic facies study of 3D seismic data, northern Louisiana, Wilcox Formation: Gulf Coast Association of Geological Societies Transactions, **62**, 73–91.

Enomoto, C. B., 2014, Well log and 2D seismic data character of the Wilcox Group in South-Central Louisiana: Gulf Coast Association of Geological Societies Transactions, **64**, 105–118.

Fatti, J. L., G. C. Smith, P. J. Vail, P. J. Strauss, and P. R. Levitt, 1994, Detection of gas in sandstone reservoirs using AVO analysis: A 3-D seismic case history using the Geostack technique: Geophysics, **59**, 1362–1376, doi: 10.1190/1.1443695.

Fisher, W. L., and J. H. McGowen, 1969, Depositional systems in Wilcox Group (Eocene) of Texas and their relation to occurrence of oil and gas: AAPG Bulletin, **53**, 30–54.

Galloway, W. E., W. F. Dingus, and R. E. Paige, 1991, Seismic and depositional facies of paleocene-eocene Wilcox group submarine canyon fills, northwest Gulf Coast, USA, *in* P. Weimer and M. H. Link, eds., Seismic facies and sedimentary processes of submarine fans and turbidite systems: Springer, 247–271.

Galloway, W. E., P. E. Ganey-Curry, X. Li, and R. T. Buffler, 2000, Cenozoic depositional history of the Gulf of Mexico basin: AAPG Bulletin, **84**, 1743–1774, doi: 10.1306/8626C37F-173B-11D7-8645000102C1865D.

Galloway, W. E., and T. A. McGilvery, 1995, Facies of a submarine canyon fill reservoir complex, lower Wilcox Group (Paleocene), central Texas coastal plain: Turbi-

Downloaded from http://pubs.geoscienceworld.org/interpretation/article-pdf/8/4/T991/5204880/int-2019-0178.1.pdf
by Missouri University of Science and Technology user

dites and Associated Deep-Water Facies, **20**, 1–23, doi: 10.2110/cor.95.20.0001.
Galloway, W. E., T. L. Whiteaker, and P. Ganey-Curry, 2011, History of Cenozoic North American drainage basin evolution, sediment yield, and accumulation in the Gulf of Mexico basin: Geosphere, **7**, 938–973, doi: 10.1130/GES00647.1.
Hampson, D. P., B. H. Russell, and B. Bankhead, 2005, Simultaneous inversion of pre-stack seismic data: 75th Annual International Meeting, SEG, Expanded Abstracts, 1633–1637, doi: 10.1190/1.2148008.
Han, D. H., A. Nur, and D. Morgan, 1986, Effects of porosity and clay content on wave velocities in sandstones: Geophysics, **51**, 2093–2107, doi: 10.1190/1.1442062.
Hargis, R. N., 1986, Proposed stratigraphic classification of the Wilcox of South Texas: Contributions to the Geology of South Texas, 135–159.
Hargis, R. N., 2009, Major transgressive shales of the Wilcox, northern portion of south Texas: South Texas Geological Society Bulletin, **49**, 19–47.
Krief, M., J. Garat, J. Stellingwerff, and J. Ventre, 1990, A petrophysical interpretation using the velocities of P and S waves (full-waveform sonic): The Log Analyst, **31**, 355–369.
Mackey, G. N., B. K. Horton, and K. L. Milliken, 2012, Provenance of the Paleocene–Eocene Wilcox Group, western Gulf of Mexico basin: Evidence for integrated drainage of the southern Laramide Rocky Mountains and Cordilleran arc: GSA Bulletin, **124**, 1007–1024, doi: 10.1130/B30458.1.
McDonnell, A., R. G. Loucks, and W. E. Galloway, 2008, Paleocene to Eocene deep-water slope canyons, western Gulf of Mexico: Further insights for the provenance of deep-water offshore Wilcox Group plays: AAPG Bulletin, **92**, 1169–1189, doi: 10.1306/05150808014.
Olariu, M. I., and W. A. Ambrose, 2016, Process regime variability across growth faults in the Paleogene Lower Wilcox Guadalupe Delta, South Texas Gulf Coast: Sedimentary Geology, **341**, 27–49, doi: 10.1016/j.sedgeo.2016.05.013.
Olariu, M. I., and H. Zeng, 2017, Prograding muddy shelves in the Paleogene Wilcox deltas, south Texas Gulf Coast: Marine and Petroleum Geology, **91**, 71–88, doi: 10.1016/j.marpetgeo.2017.12.027.
Russell, B., and D. Hampson, 2006, The old and the new in seismic inversion: CSEG Recorder, **31**, 5–11.
Sarkar, S., S. Verma, and K. J. Marfurt, 2016, Seismic-petrophysical reservoir characterization in the northern part of the Chicontepec Basin, Mexico: Interpretation, **4**, no. 3, T403–T417, doi: 10.1190/INT-2015-0168.1.
Wagner, C., A. Gonzalez, V. Agarwal, A. Koesoemadinata, D. Ng, S. Trares, N. Biles, and K. Fisher, 2012, Quantitative application of poststack acoustic impedance inversion to subsalt reservoir development: The Leading Edge, **31**, 528–537, doi: 10.1190/tle31050528.1.
Winker, C. D., 1982, Cenozoic shelf margins, Northwestern Gulf of Mexico: Gulf Coast Association of Geological Societies Transactions, **32**, 427–448.
Zeng, H., W. A. Ambrose, and W. Xu, 2016, Sediment dispersal patterns of the outer shelf to upper slope Paleocene-Eocene Wilcox Group, South-Central Texas coast: Gulf Coast Association of Geological Societies Transactions, **5**, 215–237.
Zhang, B., D. Chang, T. Lin, and K. J. Marfurt, 2014, Improving the quality of prestack inversion by prestack data conditioning: Interpretation, **3**, no. 1, T5–T12, doi: 10.1190/INT-2014-0124.1.

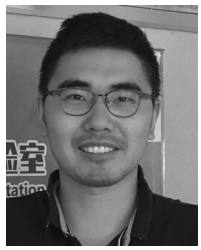

Tianze Zhang received a B.E. (2014) in resource prospecting engineering from the China University of Geosciences and a Ph.D. (2019) in geology and geophysics from the Missouri University of Science and Technology. Since his graduation, he has been teaching and conducting research at the Energy College of Chengdu University of Technology as a lecturer. His primary research interests include quantitative seismic interpretation for conventional and unconventional energy resources.

Yani Lin received a B.E. in resources prospecting engineering from the Chengdu University of Technology in 2013 and a Ph.D. in geology and geophysics from the Missouri University of Science and Technology in 2019. She has been a lecturer in the Energy College of the Chengdu University of Technology since graduation. Her primary research interests include seismic interpretation using attribute analysis.

Kelly Hong Liu is a professor of geophysics at the Missouri University of Science and Technology. She received a B.S. (1984) in exploration geophysics from the China University of Petroleum and a Ph.D. (1998) in geophysics and space physics from the University of California, Los Angeles. Her expertise includes 3D seismic data interpretation, digital signal processing and analyses, computational and observational seismology, and layered structure detection in the earth's mantle. She is an elected fellow of the Geological Society of America and an associate editor for the *Journal of Geophysical Research: Solid Earth*.

Downloaded from http://pubs.geoscienceworld.org/interpretation/article-pdf/8/4/T991/5204880/int-2019-0178.1.pdf
by Missouri University of Science and Technology user

Stephen Shangxing Gao is the chair of the Geology and Geophysics Program and a professor of geophysics at the Missouri University of Science and Technology. He received a B.S. (1984) in marine geology and geophysics from the Ocean University of China and a Ph.D. (1995) in geophysics and space physics from the University of California, Los Angeles (UCLA). He was a postdoctoral research associate at UCLA and the Carnegie Institution of Washington and served in the faculty of Kansas State University prior to joining Missouri University of Science and Technology in 2006. He is a member of SEG and the American Geophysical Union and an elected fellow of the Geological Society of America. His research interests include using P-to-S and S-to-P converted waves to image crustal and mantle discontinuities, crustal and mantle seismic anisotropy, and seismic tomography studies of the earth's interior. So far, he has published more than 100 peer-reviewed journal articles and approximately 250 conference proceedings or abstracts.

Downloaded from http://pubs.geoscienceworld.org/interpretation/article-pdf/8/4/T991/5204880/int-2019-0178.1.pdf
by Missouri University of Science and Technology user